JOURNAL OF THERMOPHYSICS AND HEAT TRANSFER
Vol. 10, No. 4, October–December 1996

Natural Convection in a Porous Cavity Saturated with a Non-Newtonian Fluid

D. Getachew,* W. J. Minkowycz,† and D. Poulikakos†
University of Illinois at Chicago, Chicago, Illinois 60607

A numerical and theoretical study is performed to analyze the steady-state natural convection fluid flow and heat transfer in a rectangular porous cavity filled with a non-Newtonian fluid and bounded by impermeable surfaces. The flow is modeled by utilizing the modified Darcy equations. Isothermal boundary conditions are considered where two opposite vertical walls are kept at constant but different temperatures, and the horizontal walls are insulated. The external parameters are the AR, *Ra*, and power-law index. Employing pure scaling arguments, four heat transfer modes are identified: 1) pure conduction, 2) high-*Ra* convection, 3) distinct horizontal boundary-layer convection, and 4) distinct vertical boundary-layer convection. The results obtained from the scaling arguments are verified numerically. The agreement between the results obtained from the scaling arguments and the numerical model is good. The numerical results are presented in terms of theoretical streamlines and isotherms, the average *Nu* at the hot wall, the horizontal velocity at the vertical midplane, the vertical velocity at the horizontal midplane, and the temperature distribution at the horizontal and the vertical midplanes.

Nomenclature

c_{p_f} = specific heat of the fluid
Da = Darcy's number
Fs = Forchheimer number
g = magnitude of the gravity vector
$\boldsymbol{g}$ = gravitational body force
H = total height of the cavity
i, j = indices
k''' = effective thermal conductivity of the porous medium
L = total length of the cavity
m = consistency index
Nu = Nusselt number
n = flow behavior index
Pr = Prandtl number
q = heat transfer per unit depth
$\boldsymbol{q}_f$ = heat flux in the fluid phase
Ra = modified Rayleigh number
S = source term
T = dimensionless temperature
T_s = temperature
u, v = dimensionless velocity components
u_f, v_f = velocity components
$\boldsymbol{v}$ = velocity vector
x, y = dimensionless coordinates in the physical domain
$\bar{x}, \bar{y}$ = coordinates in the physical domain
Y = correction factor
α_m = thermal diffusivity of the porous medium
β = volumetric expansion coefficient
Γ = generalized diffusion coefficient
ρ_f = density of the fluid
ϕ = general dependent variable
ψ = stream function

Subscripts
cond = conduction heat transfer
conv = convection heat transfer
f = properties in the fluid phase
s = properties in the solid phase

Received July 6, 1995; revision received Feb. 28, 1996; accepted for publication April 18, 1996.

*Department of Mechanical Engineering; currently Associate Professor, Department of Mathematics and Computer Science, Chicago State University, Chicago, IL 60628.
†Professor, Department of Mechanical Engineering.

Introduction

INTEREST in natural convection fluid flow and heat transfer in porous media has been motivated by a broad range of applications, including geothermal systems, crude oil production, storage of nuclear waste material, ground water pollution, etc. A comprehensive review of the literature is available.[1] In a wide variety of such problems the physical system can be modeled as a two-dimensional rectangular enclosure filled with a homogeneous porous medium, with the vertical walls at different temperatures and the connecting horizontal walls being considered adiabatic.

In the past two decades, numerous theoretical and experimental investigations have been devoted to the steady-state natural convection flow and heat transfer in such enclosures.[1-18] Theoretical works reported include numerical results,[2-9] boundary-layer analyses,[2-9] and important experimental results.[10,11] Based on these studies, various correlations have been reported for the average Nusselt number for shallow, square, and tall cavities.

With the exception of Chan et al.,[2] who considered the viscous diffusion effects, most of the early theoretical studies were based on Darcy's law. An excessive effort has taken place over the past decade to study non-Darcy effects (flow inertia and viscous diffusion) on natural convection in an enclosed porous layer.[12-19] No details of those studies are discussed herein for brevity.

The fluids that have been used in all of the previously mentioned investigations were Newtonian fluids. Thus, from the viewpoint of theoretical analysis, the work with Newtonian fluids has received the maximum attention and is well understood. On the other hand, for non-Newtonian fluids, to the best of the authors' knowledge, with the exception of the works of Bian et al.,[20,21] no work on natural convection in a rectangular porous cavity saturated with a non-Newtonian fluid has been reported. All of the existing literature on natural convection in a porous medium saturated with non-Newtonian fluids is for external flows over various surfaces.[22-28] An exhaustive listing on this subject may be found in the article by Shanoy.[29]

The purpose of this article is to analyze the behavior of a natural convection flow in a rectangular porous material saturated with a non-Newtonian fluid. The problem is analyzed

numerically, for two-dimensional flow patterns, via the finite difference solution of the governing equations. The flow is modeled by utilizing the Darcy equation for the porous layer.

Formulation of the Problem

Problem Considered

Consider a natural convection in an enclosed porous medium with rectangular impermeable boundaries. The porous medium is assumed to be saturated with a purely viscous non-Newtonian fluid of the Ostwald-de Waele power-law type. The configuration is shown in Fig. 1. The side walls are of height H and at distance L apart. They are maintained at temperatures T_h and T_c, with $\Delta T = T_h - T_c > 0$. The top and bottom walls are considered perfectly insulated. The coordinate system is defined so that the vertical axis points vertically upward in the direction opposite to the gravity vector of magnitude $\boldsymbol{g}$. The x axis is horizontal.

Heat transfer through the walls causes density changes to the fluid in the cavity and leads to the buoyancy-driven recirculation. The resulting flow is treated as steady, laminar, and two dimensional. Furthermore, in the formulation of the problem, it has been assumed that the fluid properties are constant, except for the density variation in producing the buoyancy force; viscous drag and inertia terms are neglected; velocity slip at the bounding surface is permitted; and the viscous heat dissipation, the compression work, and the heat generation are assumed to be neglected.

Differential Equations

With the previous assumptions, the macroscopic forms of the governing equations, extracted from the general macroscopic equations obtained from the corresponding microscopic equations with the method of volume averaging[30,31] for the case of Darcy's flow, are

$$\frac{\partial u_f}{\partial \bar{x}} + \frac{\partial v_f}{\partial \bar{y}} = 0 \tag{1}$$

$$\frac{mY}{\kappa}\frac{\partial}{\partial \bar{y}}\left(|\boldsymbol{v}_f|^{n-1}u_f\right) - \frac{mY}{\kappa}\frac{\partial}{\partial \bar{x}}\left(|\boldsymbol{v}_f|^{n-1}v_f\right) = -\rho_f g\beta\frac{\partial T_f}{\partial \bar{x}} \tag{2}$$

$$u_f\frac{\partial T_f}{\partial \bar{x}} + v_f\frac{\partial T_f}{\partial \bar{y}} = \frac{\partial}{\partial \bar{x}}\left(\alpha_m\frac{\partial T_f}{\partial \bar{x}}\right) + \frac{\partial}{\partial \bar{y}}\left(\alpha_m\frac{\partial T_f}{\partial \bar{y}}\right) \tag{3}$$

where

$$|\boldsymbol{v}_f| = (u_f^2 + v_f^2)^{1/2} \tag{4a}$$

$$\alpha_m = \frac{k'''}{c_{p_f}\rho_f} \tag{4b}$$

Note that Eq. (2) is obtained after eliminating the pressure p by cross differentiating and subtracting the x and y momentum equations. The power-law exponent of the non-Newtonian fluid is denoted by n. The modified permeability of the porous matrix saturated with non-Newtonian fluid is[31]

$$\kappa = \frac{d_p^{n+1}\varepsilon_f^{n+2}}{180(1-\varepsilon_f)^2}$$

where ε_f is the porosity and d_p is the average pore diameter. The correction factor Y is a function of the power-law index.[31]

Boundary Conditions

To complete the mathematical formulation of the enclosure convection problem, the boundary conditions for the governing differential equations need to be specified. The relevant hydrodynamic and thermal boundary conditions are as follows:

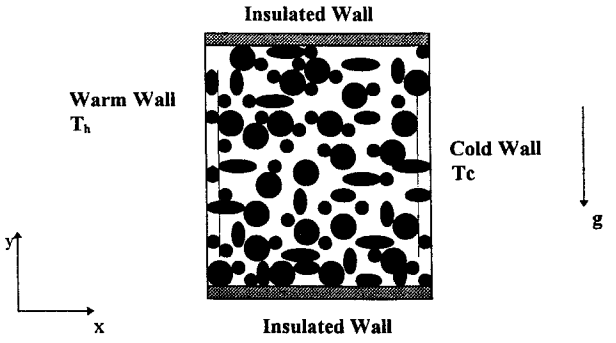

Fig. 1 Two-dimensional rectangular porous layer held between differentially heated walls.

Impermeable walls:

$$u_f = 0 \quad \text{at} \quad \bar{x} = 0, L \tag{5a}$$

$$v_f = 0 \quad \text{at} \quad \bar{y} = 0, H \tag{5b}$$

Adiabatic top and bottom boundaries:

$$\frac{\partial T}{\partial \bar{y}} = 0 \tag{6a}$$

at

$$\bar{y} = 0, H \tag{6b}$$

Constant-temperature side walls:

$$T = T_h \quad \text{at} \quad \bar{x} = 0 \tag{7a}$$

$$T = T_c \quad \text{at} \quad \bar{x} = L \tag{7b}$$

The flow and temperature fields in the porous layer can be obtained by solving Eqs. (1–3), subject to the boundary conditions given by Eqs. (5–7).

Method of Solution

The problem formulated in the preceding section is studied by using two different methods: 1) analytical and 2) numerical. The analytical method utilizes the pure scaling arguments[32] to estimate, in an order-of-magnitude sense, the type of flow and heat transfer pattern that can develop in the enclosure. The results obtained using the scaling arguments are then verified by performing a series of numerical experiments. The numerical method used to solve the governing equations is based on finite differences.[31,33,34] The implementation of these two methods for solving the aforementioned problem will be discussed in the following subsections.

Scale Analysis

To obtain the scaling results, consideration was given to the region of thickness δ and height H that is shown in Fig. 1. In this region, using the scales $x \sim \mathcal{O}(\delta)$, $y \sim \mathcal{O}(H)$, and $T \sim \mathcal{O}(\Delta T)$, the order-of-magnitude equivalent of Eqs. (1) and (3) (Ref. 32) is

$$(u/v) \sim (\delta/H) \tag{8}$$

$$(u/\delta)\Delta T + (v/H)\Delta T \sim (\alpha_m\Delta T/\delta^2) + (\alpha_m\Delta T/H^2) \tag{9}$$

Combining Eqs. (8) and (9)

$$(v/H)\Delta T \sim \alpha_m(\Delta T/\delta^2)[1 + (\delta/H)^2] \tag{10}$$

Furthermore, from Eq. (2)

$$(u/H)|v|^{n-1} - (v/\delta)|v|^{n-1} \sim (\rho g \beta \kappa / mY)(\Delta T/\delta) \quad (11)$$

Using the fact that

$$|v| \sim \mathcal{O}[v\sqrt{(\delta/H)^2 + 1}] \quad (12)$$

Eq. (11) yields

$$(v/\delta)[v\sqrt{(\delta/H)^2 + 1}]^{n-1}[(\delta/H)^2 - 1] \sim (\rho g \beta \kappa / mY)(\Delta T/\delta) \quad (13)$$

Since $\delta \times H$ is a boundary layer, we may assume $\delta << H$. Based on the previous equation, the scales for the vertical boundary layers in the cavity are

$$v \sim (\alpha_m/HY^{1/n})Ra^{1/n} \quad (14)$$

$$\delta \sim HY^{1/2n}R_a^{-(1/2n)} \quad (15)$$

$$u \sim (\alpha_m/H)(1/Y^{1/2n})Ra^{1/2n} \quad (16)$$

where Ra is the modified Darcy–Rayleigh number, for non-Newtonian flow, based on the height of the cavity

$$Ra = \rho g \beta \kappa H^n \Delta T / m \alpha_m^n \quad (17)$$

The heat transfer rate per unit depth is

$$q = Hk_m \left(\frac{\partial T}{\partial x}\right)_{x=0} \quad (18)$$

The order-of-magnitude equivalent of this equation reads

$$q \sim (k_m \Delta T/Y^{1/2n})Ra^{1/2n} \quad (19)$$

Using the heat transfer in the pure conduction limit $q_c = k_m H \Delta T/L$ as a reference quantity, the overall Nusselt number is derived as

$$Nu = (q/q_c) \sim (1/Y^{1/2n})(L/H)Ra^{1/2n} \quad (20)$$

The scaling analysis presented previously may be utilized to set criteria for distinguishing distinct thermal boundary layers, as discussed[32] for Newtonian fluids.

Criterion for Distinct Vertical Boundary Layers

The requirement to have a distinct vertical boundary layer is $\delta << L$. From Eq. (15)

$$(\delta/H) \sim (Y/Ra)^{1/2n} \quad (21)$$

Therefore, the requirement to have distinct vertical boundary layers is that

$$(H/L) << (Ra/Y)^{1/2n} \quad (22)$$

Criterion for Distinct Horizontal Boundary Layers

Following the arguments in Bejan,[32] the two horizontal jets form a counterflow that carries energy by convection from one vertical wall to the other. Let this heat transfer by convection be denoted by q_{conv}, where

$$q_{conv} = \mathcal{Q}(\rho c_p)\Delta T \quad (23)$$

The volume flow rate per unit depth is $\mathcal{Q} \sim \mathcal{O}(v\delta)$. Thus, the order of magnitude equivalent of the previous equation is

$$q_{conv} \sim v\delta(\rho c_p)\Delta T \quad (24)$$

Let the heat transfer rate per unit depth between the two horizontal jets be denoted by q_{cond}, where

$$q_{cond} = -k_m L \frac{\partial T}{\partial y} \quad (25)$$

The order of magnitude equivalent of this equation is

$$q_{cond} \sim k_m L(\Delta T/H) \quad (26)$$

The criterion for distinct horizontal boundary layer is

$$q_{cond} << q_{conv} \quad (27)$$

which leads to

$$(H/L) >> Y^{1/2n}Ra^{-(1/2n)} \quad (28)$$

Table 1 Expressions for Γ and S for various dependent variables

ϕ	Γ	S
ψ	$Y(\sqrt{u^2 + v^2})^{n-1}$	$Ra\,\frac{\partial T}{\partial x}$
T	1	0

Table 2 Overall *Nu* at the hot wall for various nonuniform grids

Ra	22 × 22	32 × 32	42 × 42	Ref. 8
25	1.35	1.34	1.37	1.38
50	1.92	1.95	1.96	1.98
100	2.98	3.04	3.07	3.097
500	8.10	8.48	8.65	8.66
1000	11.8	12.6	12.9	12.96

Table 3 Summary of numerical experiments on natural convection in the effect of n^a

	n		
A	0.56	0.78	1.00
0.25	8.53	4.38	3.09
1.00	10.30	4.74	3.07
4.00	3.40	1.62	1.22

[a]The overall *Nu* at the hot wall (*Ra* = 100).

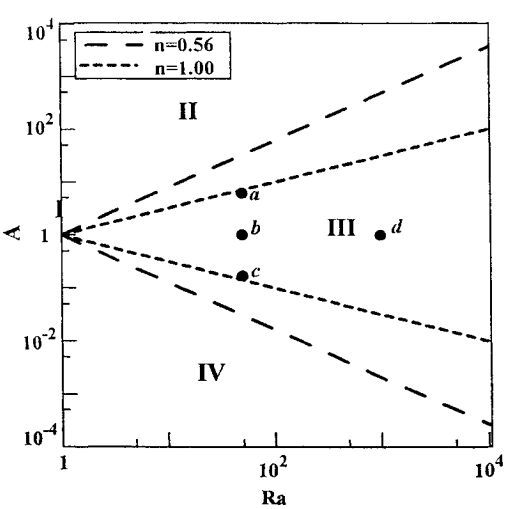

Fig. 2 Flow regimes as defined by the scaling criteria.

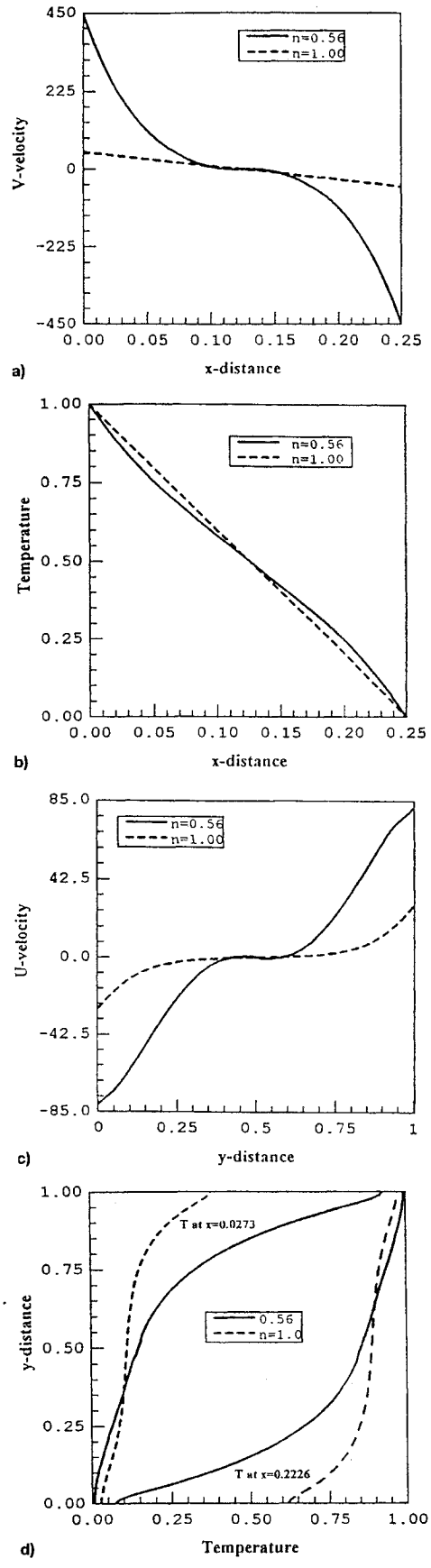

Fig. 3 Non-Newtonian effect for $Ra = 100$ and $A = 4.0$: a) vertical velocity profiles at the horizontal midplane, b) temperature distribution at the horizontal midplane, c) horizontal velocity profile at the vertical midplane, and d) temperature distribution at the two vertical planes near the two side walls.

Convection Regime

From the previous considerations it is evident that, because of the dimensionless parameters that govern the phenomenon, namely, *Ra*, the geometric AR, and the power-law index *n*, there are different flow regimes that are possible in the configuration of Fig. 1. For a fixed value of *n*, the scale analysis shows that these possible flow regimes occupy well-defined regions in the two-dimensional domain $(H/L) - Ra$. These regimes, which characterize the heat transfer for natural convection in a two-dimensional enclosure heated from the side, are summarized in Fig. 2. Thus, for a fixed value of *n*, as discussed for Newtonian fluids by Poulikakos and Bejan,[14] the results derived in this section suggest the following four possibilities: 1) pure conduction (no distinct boundary layers), 2) high *Ra* convection (distinct horizontal and vertical boundary layers), 3) tall layers (distinct horizontal boundary layers

Table 4 Summary of numerical experiments on natural convection in the effect of *A* and *Ra*[a]

	A		
Ra	0.25	1.00	4.00
1.00	0.99	0.99	0.99
50.00	2.06	4.21	1.45
100.00	4.38	4.74	1.62

[a]The overall *Nu* at the hot wall ($n = 0.78$).

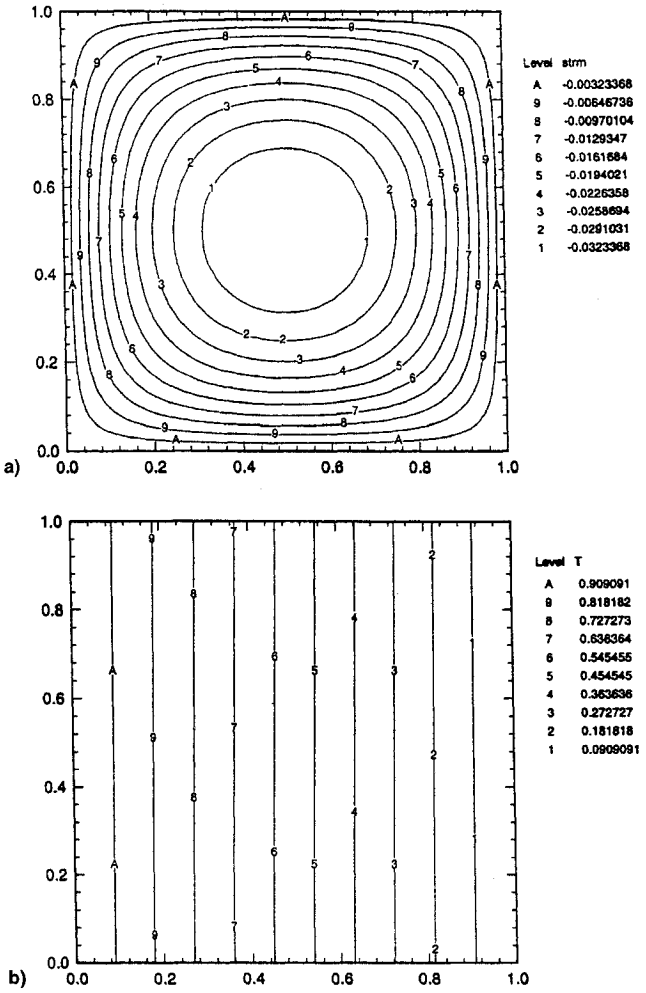

Fig. 4 Results for $n = 0.78$, $A = 1.0$, and $Ra = 1.0$: a) streamline and b) isotherms.

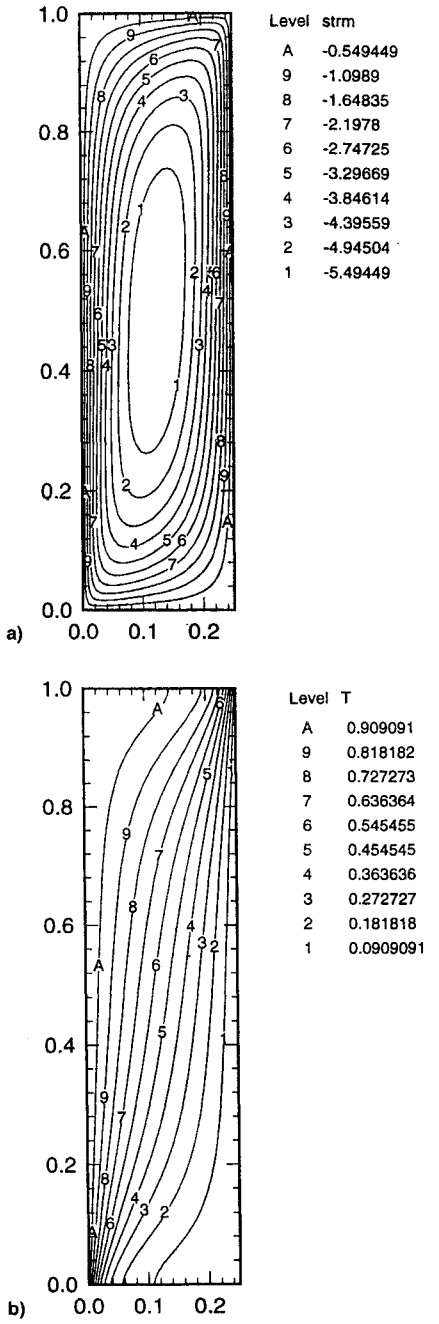

Fig. 5 Results for n = 0.78, A = 4.0, and Ra = 100.0: a) streamlines and b) isotherms.

only), and 4) shallow layers (distinct vertical boundary layers only).

One interesting result observed from the scale analysis is that the region for high Ra convection gets wider as the value of n decreases from its Newtonian value. Thus for a fixed value of Ra there is a value of $A > 1$ (or $A < 1$), where decreasing n from its Newtonian value will change the flow structure from tall layer limit (or shallow layer limit) to high Ra convection regime. In the following section these results will be verified on the basis of numerical simulations.

Numerical Method

Nondimensionalization

The numerical solution is aided somewhat by rewriting the governing equations [Eqs. (1–7)], in a nondimensional form. To nondimensionalize these equations, we introduce the characteristic values H, α_m/H, and $\Delta T = T_h - T_c$ to denote the

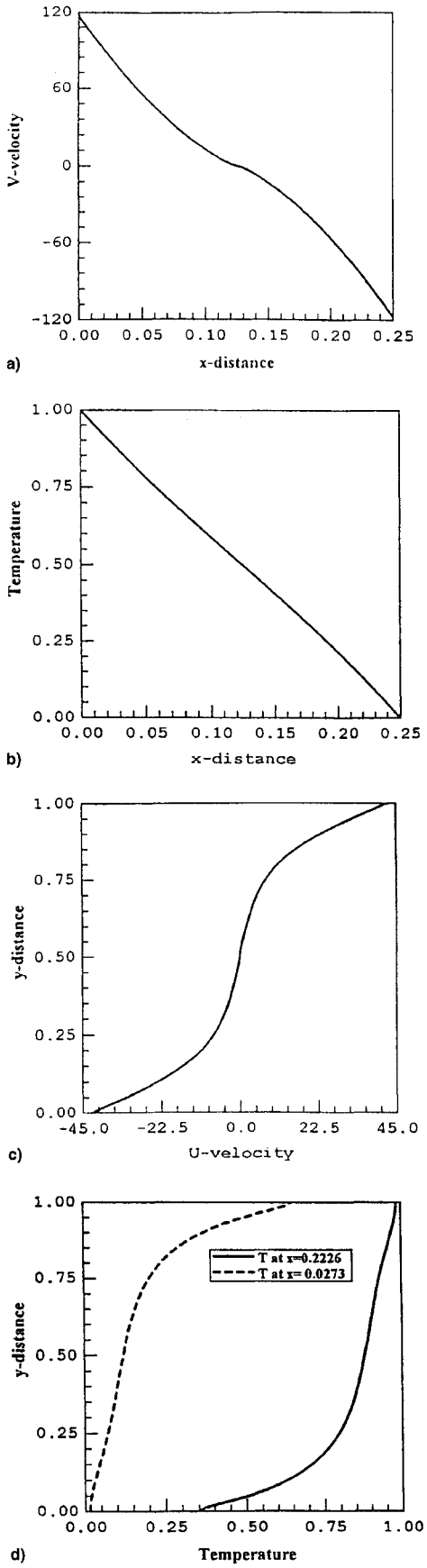

Fig. 6 Results for n = 0.78, A = 4.0, and Ra = 100.0: a) vertical velocity profiles at the horizontal midplane; b) temperature distribution at the horizontal midplane, c) horizontal velocity profile at the vertical midplane, and d) temperature distribution at the two vertical planes near the two side walls.

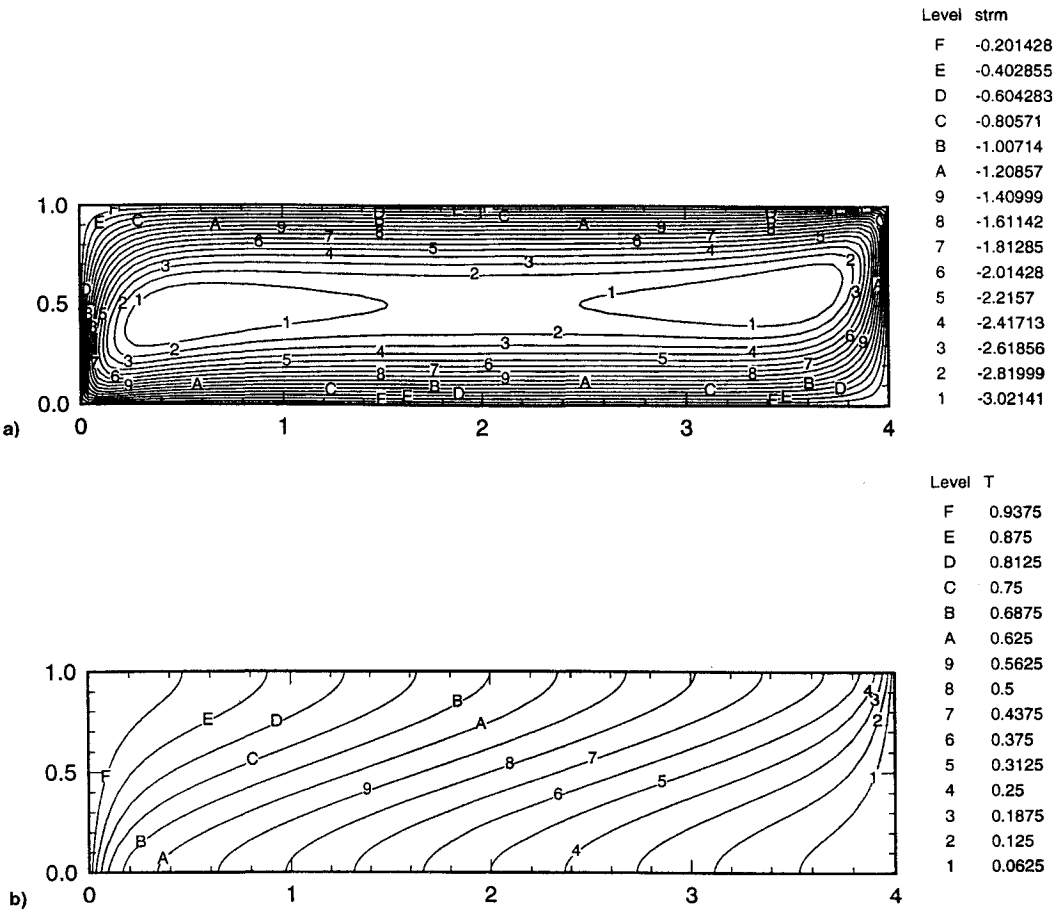

Fig. 7 Results for $n = 0.78$, $A = 0.25$, and $Ra = 100.0$: a) streamlines and b) isotherms.

reference values of length, velocity, and temperature, respectively. To denote the dimensionless dependent variables, the subscript f is dropped. Thus,

$$u = u_f/(\alpha_m/H) \tag{29a}$$

$$T = (T_f - T_c)/(T_h - T_c) \tag{29b}$$

$$v = v_f/(\alpha_m/H) \tag{29c}$$

The dimensionless independent variables are taken as

$$x = \bar{x}/H \tag{30a}$$

$$y = \bar{y}/H \tag{30b}$$

Using these transformations, the governing equations for the case of Darcy's flow can be written in a nondimensional form as

$$0 = \frac{\partial}{\partial x}\left(Y|\boldsymbol{v}|^{n-1}\frac{\partial \psi}{\partial x}\right) + \frac{\partial}{\partial y}\left(Y|\boldsymbol{v}|^{n-1}\frac{\partial \psi}{\partial y}\right) + Ra\frac{\partial T}{\partial x} \tag{31}$$

$$\frac{\partial(uT)}{\partial x} + \frac{\partial(vT)}{\partial y} = \frac{\partial^2 T}{\partial x^2} + \frac{\partial^2 T}{\partial y^2} \tag{32}$$

where

$$u = \frac{\partial \psi}{\partial y} \tag{33}$$

$$v = -\frac{\partial \psi}{\partial x} \tag{34}$$

The boundary conditions are

$$u = 0 \tag{35a}$$

$$\psi = 0 \tag{35b}$$

$$T = 1 \quad \text{at} \quad x = 0 \tag{35c}$$

$$u = 0 \tag{36a}$$

$$\psi = 0 \tag{36b}$$

$$T = 0 \quad \text{at} \quad x = L/H \tag{36c}$$

$$v = 0 \tag{37a}$$

$$\psi = 0 \tag{37b}$$

$$\frac{\partial T}{\partial y} = 0 \quad \text{at} \quad y = 0, 1 \tag{37c}$$

In the previous equations

$$|\boldsymbol{v}| = \sqrt{u^2 + v^2} \tag{38}$$

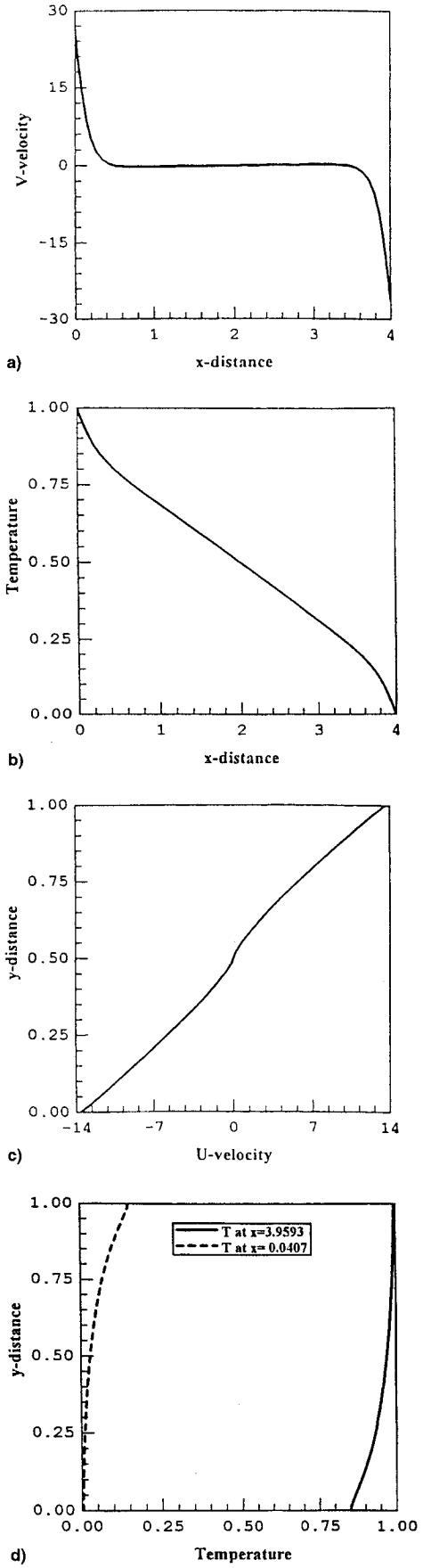

Fig. 8 Results for $n = 0.78$, $A = 0.25$, and $Ra = 100.0$: a) vertical velocity profiles at the horizontal midplane, b) temperature distribution at the horizontal midplane, c) horizontal velocity profile at the vertical midplane, and d) temperature distribution at the two vertical planes near the two side walls.

and Ra is given by Eq. (17). The details of the derivation of these equations is presented in Ref. 31.

Numerical Procedure

The computation of ψ and T from Eqs. (31) and (32) is mathematically identical to solving

$$\frac{\partial(\lambda u\phi)}{\partial x} + \frac{\partial(\lambda v\phi)}{\partial y} = \frac{\partial}{\partial x}\left(\Gamma \frac{\partial \phi}{\partial x}\right) + \frac{\partial}{\partial y}\left(\Gamma \frac{\partial \phi}{\partial y}\right) + S \quad (39)$$

In this equation λ is a parameter that assumes a value equal to one for the temperature equation and zero of the stream function equation. When a particular meaning is associated with ϕ, the expressions for Γ and S are then obtained by comparing the actual conservation equation for the chosen variable with Eq. (39). A complete list of Γ and S for different dependent variables used here is given in Table 1.

A detailed description of the numerical method used for solving the general differential equation is omitted here for brevity.[31] Only a brief summary is presented herein.

The discretization equations are derived employing a numerical method that is based on the control volume formulation.[33-36] The resulting system of algebraic equations is solved iteratively, using the line-by-line method idea proposed by Patankar.[33]

Starting with estimated or guessed values for ψ, we first solve for the velocity components u and v from Eqs. (33) and (34); the resulting u and v fields are then used for the convection term in the temperature equation to calculate the temperature distribution. Once the values of T are obtained, the results are used for the source term in the stream function equation. At this point we check if the criterion for convergence is satisfied. If not, we repeat the cycle by calculating the velocity components from the current estimated values of the stream function.

Two criteria, pointwise convergence for the temperature and stream function fields and global convergence for the total heat flux at the hot wall, were applied in this study. The total heat flux was considered to have converged when no change occurred in the first four significant figures for three consecutive iterations. Typically, pointwise convergence was achieved, depending on Ra, in about 40–400 iterations.

The criterion used for iterative convergence was

$$\frac{\sum_{i,j} |(\phi_{i,j})_{\text{new}} - (\phi_{i,j})_{\text{old}}|}{\sum_{i,j} |(\phi_{i,j})_{\text{new}}|} < r_f$$

where r_f has been taken as 10^{-4} for both ψ and T.

Validation of Numerical Solution

All computations reported in this study were performed on the IBM RISC/6000 Aix Version 3.2 computer. To test the accuracy of the numerical algorithm, we compared the present results to those reported in the literature for the limiting case of Newtonian fluid flow in porous media. The results of these comparisons are given in Table 2. The table presents the numerical predictions of the overall Nusselt numbers at the hot wall obtained with different grid sizes for various values of Ra along with the corresponding analytical results obtained by Walker and Homsy.[8] It is evident from the table that the 32 $\times$ 32 grid provides satisfactory results for $Ra \leq 100$, whereas the 42 $\times$ 42 grid is sufficient for higher values of Ra. Thus, to be on a safe side, for all of the numerical experiments presented in this article, a grid of 42 $\times$ 42 nodal points is used.

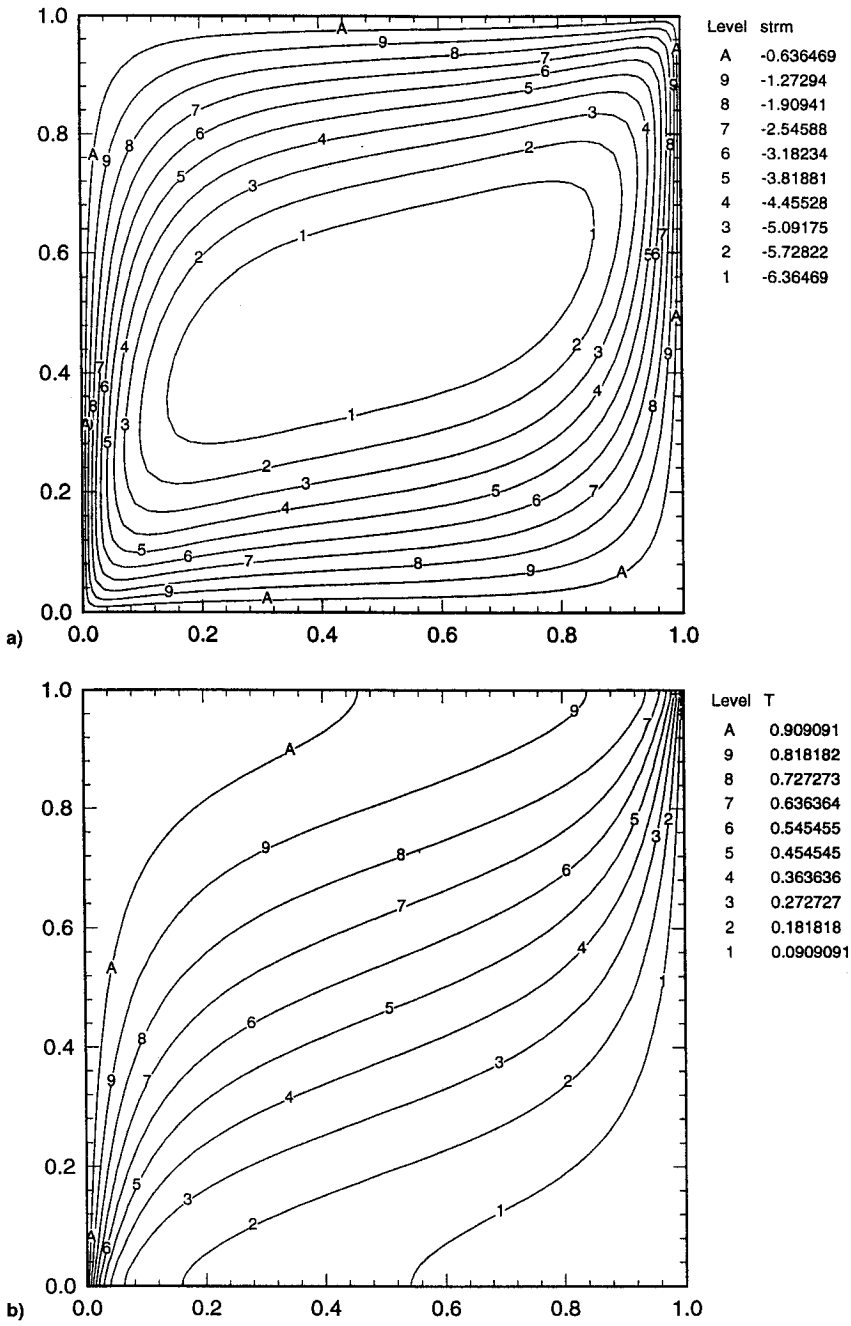

Fig. 9 Results for $n = 0.78$, $A = 1.0$, and $Ra = 100.0$: a) streamlines and b) isotherms.

Results and Discussion

The scale analysis presented in the preceding section showed that for a given flow behavior index the convection heat transfer in a porous cavity can be classified as belonging to either the conduction, tall-, boundary-, or the shallow-layer flow regime. In Fig. 2, these flow regimes are identified as I, II, III, or IV, respectively. Each of the regimes has its own characteristics and depends on the parameters associated with the problem: Ra, AR, and n. By varying one of these parameters, while fixing the other two, we may observe a change in the flow regions. For example, it can be observed that for small values of Ra, energy is transported to the cold wall by pure conduction, and Nu is unity. This situation is achieved for $Ra \rightarrow 0$ and is referred to as the conduction regime.

For the range of conditions used in this investigation, a sufficiently large Ra causes a boundary-layer flow, irrespective of n and A, in which the dominant mode of heat transfer is convection. For the case of the boundary-layer limit with $Ra \rightarrow \infty$, it is expected that thin boundary layers will form along the walls. Thus, all points in this region correspond to the case where all four boundary layers are distinct.

Another interesting feature revealed by the scale analysis is that the variation of the flow behavior index, for fixed values of Ra and A, also changes the flow structure. For example, for a given value of Ra it is possible to find a cavity with the geometric AR greater than one where a reduction in the flow behavior index changes the flow structure: tall layer $\rightarrow$ boundary layer. Similarly, it is also possible to find values of A less than one where decreasing the values of n results in changing the flow structure from shallow layer $\rightarrow$ boundary layer.

Temperature and Velocity Fields

The theoretical scaling trends predicted in the preceding section are utilized as the task of selecting the best cases for direct numerical simulation. In the first series of numerical solutions

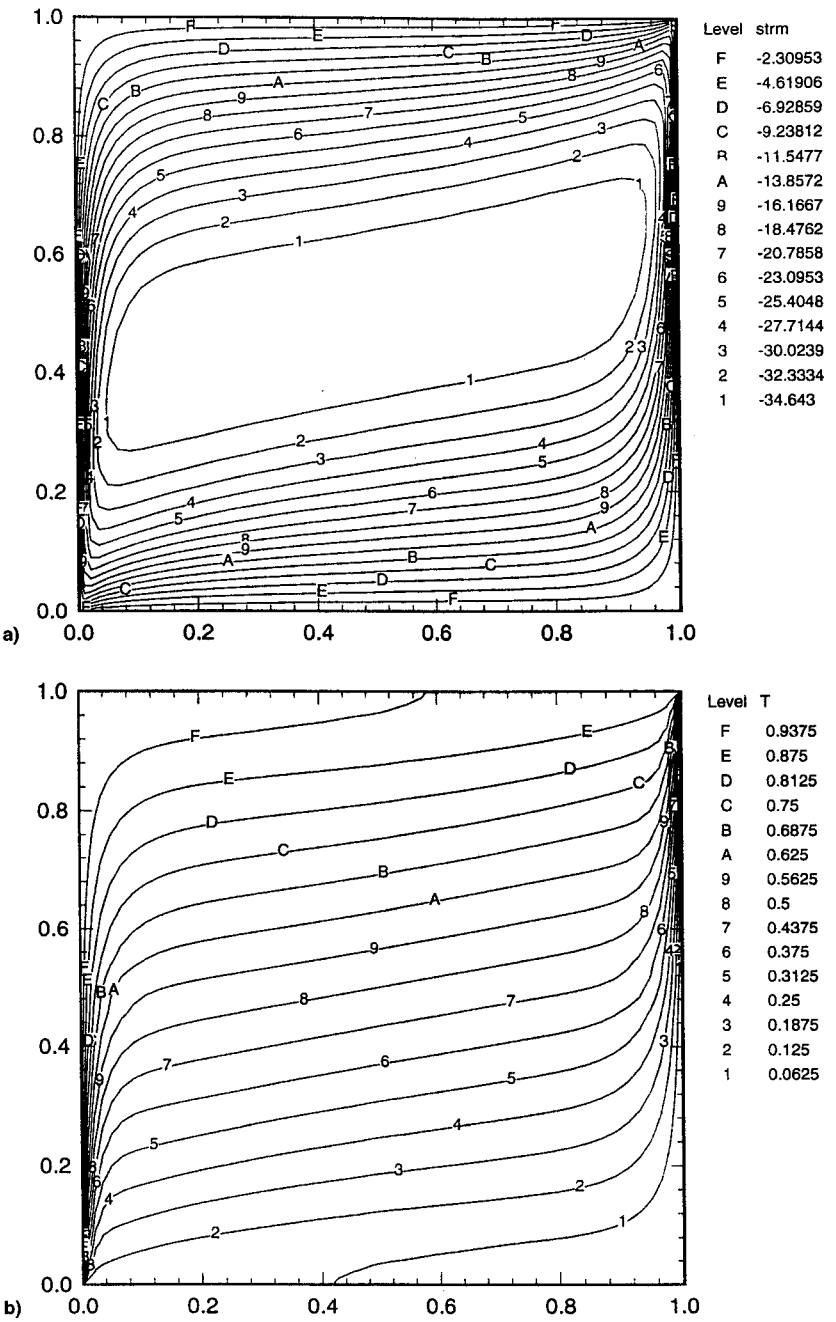

Fig. 10 Results for $n = 0.78$, $A = 1.0$, and $Ra = 800.0$: a) streamlines and b) isotherms.

obtained in this study, and summarized in Table 3, we investigated the influence of the power-law index in the heat transfer-driven flow.

To document the effect of n, the solution for Nu (for Ra = 100.00 and for three different values of the geometric AR) are summarized in Table 3. In all of these situations the Nu decreases as the flow behavior index increases. Thus, the most striking effect of increasing the power-law index towards its Newtonian value ($n = 1.0$) is the suppression of convection as a transport mechanism. This effect can be observed clearly from the results presented for the case where $A = 4.00$, which is point a in Fig. 2. This point corresponds to the flow where $A \approx (Ra/Y)^{1/2n}$, in an order-of-magnitude sense, when the fluid is Newtonian; whereas, when the fluid is non-Newtonian the point (a in Fig. 2) corresponds to the flow where $A << (Ra/Y)^{1/2n}$. Thus, as predicted via scale analysis, at point a the flow should have a tall-layer structure when $n = 1$ and a boundary-layer structure when $n < 1$. This aspect is illustrated by the sequences of temperature distribution at the vertical midplane, the temperature distribution at the horizontal midplane, the horizontal velocity u at the vertical midplane, and the vertical velocity v at the horizontal midplane displayed in Fig. 3. Clearly, Figs. 3a–3d verified the trends predicted via the scale analysis.

Table 4 summarizes the series of experiments designed to document the effect of the geometric AR and Ra. (The results are presented in Figs. 5–10.) For each case, we report the variation of 1) temperature distribution at the vertical midplane, 2) temperature distribution at the horizontal midplane, 3) u at the vertical midplane, and 4) v at the horizontal midplane. The computations are performed for the following range of conditions: $1.0 \leq Ra \leq 100$, $0.25 \leq A \leq 4.0$, and $0.55 \leq n \leq 1$. Flow patterns and temperature fields for typical values of Ra are presented.

Conduction Flow Regime

The scaling regime I defined in Fig. 2 is relevant in this case. The streamlines and isotherms for this regime are pre-

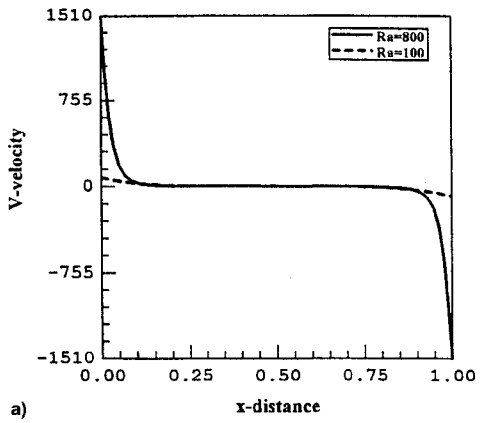

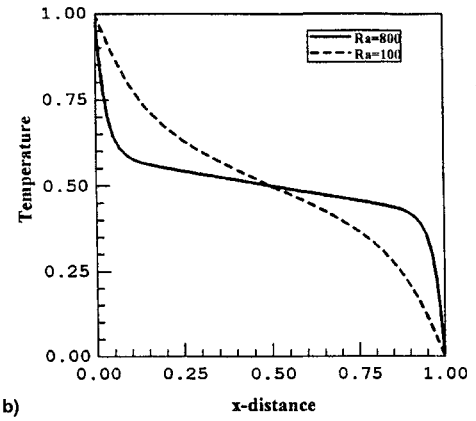

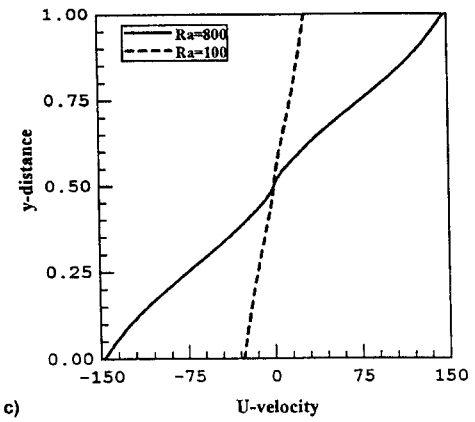

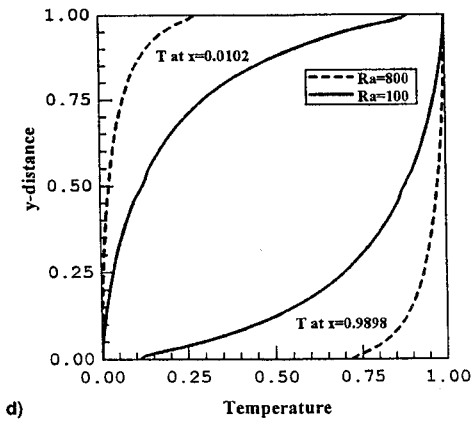

Fig. 11 Results for n = 0.78, A = 1.0, Ra = 100 and 800.0: a) vertical velocity profiles at the horizontal midplane, b) temperature distribution at the horizontal midplane, c) horizontal velocity profile at the vertical midplane, and d) temperature distribution at the two vertical planes near the two side walls.

Table 5 Numerical results for the overall Nu at the hot wall for A = 1.0

	n				
Ra	0.55	0.7	0.8	0.9	1.0
1	0.99	0.99	0.99	0.99	1.00
10	1.05	1.06	1.06	1.07	1.07
50	4.40	2.97	2.47	2.16	1.97
100	10.50	5.90	4.45	3.59	3.07
200	21.00	11.10	7.88	5.99	4.99

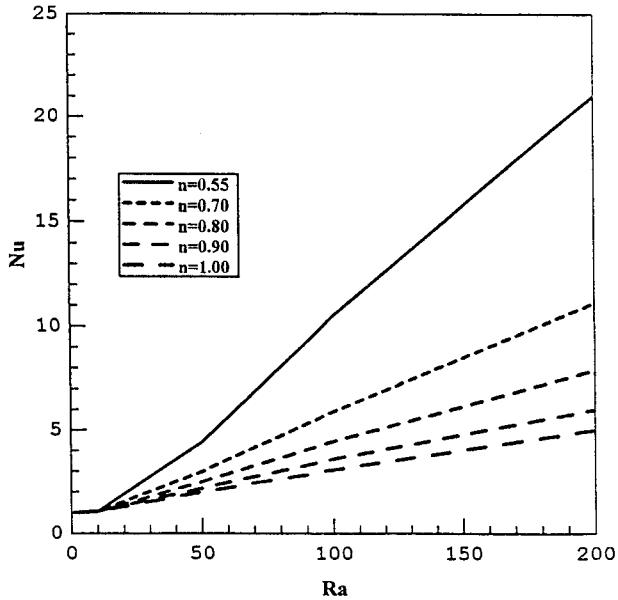

Fig. 12 Nu vs Ra, A = 1.0.

sented in Figs. 4a and 4b, respectively. In this region, the circulating convective motion is very slow and heat transfer across the enclosure is dominated by conduction. This state is characterized by vertical isotherms and a weak clockwise circulation driven by the finite $\partial T/\partial x$ gradient. From the numerical results it is observed that, for Ra = 1, the streamlines indicate the existence of a single vortex with its center in the center of the domain, as shown in Fig. 4a. The corresponding isotherms (see Fig. 4b) are parallel to the heated walls, indicating that most of the heat transfer is by heat conduction. This is in agreement with the scaling prediction made at the beginning of this section.

Tall Enclosure Limit

In Fig. 2, point a corresponds to the tall enclosure limit. To demonstrate the theoretical arguments presented in the preceding section, numerical computations are performed for Ra = 100 and A = 4.0. Figures 5a and 5b show the streamlines and the isotherm patterns, respectively, for n = 0.7, Ra = 100, and A = 4.0. From the numerical results presented in Fig. 5b, it is observed that for most of the enclosure height the isotherms are parallel to the vertical walls, indicating that most of the heat transfer is by heat conduction. This can be seen clearly from the results depicted in Figs. 6a and 6b, which are the vertical velocity and the temperature profiles, respectively, at the horizontal midplane.

The absence of a sharp temperature and velocity gradients in the vicinity of the vertical walls implies that in the neighborhood of the horizontal midplane, the heat transfer from the hot wall to the cold wall is mainly by conduction. The variation of the horizontal velocity at the vertical midplane is shown in Fig. 6c. From this result it can be observed that the horizontal velocity has the highest gradient near the horizontal walls, indicating the presence of horizontal fluid jets along these walls. These fluid

jets are responsible for the fact that the isotherms (see Fig. 5b) in the vicinity of the top and the bottom walls appear swept horizontally to the right at the top wall and to the left at the bottom wall. The results presented in Fig. 6c, along with the temperature profiles at the vertical midplane shown in Fig. 6d, indicate the presence of two distinct horizontal boundary layers. These observations are in excellent agreement with the scaling predictions made in the preceding section.

Shallow Layer

The streamlines and the isotherms for the scaling regime IV, point c in Fig. 2, are presented in Figs. 7a and 7b. For this regime, the numerical results show that the isotherms are not parallel to the vertical walls. This indicates that convection contributes to the heat transfer process. The corresponding vertical velocity distribution and temperature profiles at the horizontal midplane are depicted in Figs. 8a and 8b. Figure 8a shows that v exhibits its steepest gradients near the two vertical walls, indicating the existence of two distinct boundary layers. However, the temperature distribution at the horizontal midplane does not show a steep temperature gradient near the vertical walls. A logical explanation for this result is that because of the relatively low Ra used in the computation, the flow circulation is weak, and consequently, the cavity is dominated by a horizontal counterflow in which the two branches are in very good thermal contact. Thus, heat transfer by conduction in the vertical direction is still important. The velocity u at the vertical midplane is presented in Fig. 8c. The result shows an almost linear variation of u along the vertical midplane indicating the absence of distinct horizontal boundary layers. This can also be observed clearly from Fig. 8d, where the temperature distribution at the vertical midplane is presented. In summary, Figs. 7a–8d show the existence of distinct vertical boundary layers and the absence of distinct horizontal boundary layers, which is in agreement with the scaling predictions.

Four Boundary Layers

Theoretically, as briefly discussed at the beginning of this section, an increase in Ra (for fixed values of n and A) or a reduction in A (for fixed values of n and Ra) changes the flow structure from tall-layer limit to boundary-layer limit. In the boundary-layer regime, unlike in the last two regimes, the scaling results predict the coexistence of the horizontal and vertical boundary layers. To investigate the validity of the theoretical prediction computations were performed for $Ra = 100$, 800 and $A = 1$, shown as point b in Fig. 2. The results are shown in Figs. 9 and 10. The streamlines and the isotherms are presented in Figs. 9a and 9b. The vertical velocity distributions at the horizontal midplane (Fig. 11a), show its largest gradient near the vertical walls, indicating the existence of distinct vertical boundary layers. This is also shown in Fig. 11b by means of the temperature profiles at the horizontal midplane. Figure 11c shows the horizontal velocity distribution. The velocity distribution presented in this figure shows its largest gradient in the vicinity of the top and the bottom walls, indicating the development of distinct horizontal boundary layers. The temperature profiles at the vertical midplane are depicted in Fig. 11d. Thus, the numerical results in Figs. 9a–11d agree with the trend of the scaling predictions.

Heat Transfer

The effect of fluid motion on heat transfer between the two vertical walls of the enclosure was calculated by computing the conduction-referenced Nu

$$Nu = Q/k'''H[(T_h - T_c)/L] \tag{40}$$

where Q is the overall heat transfer rate. In terms of dimensionless quantities [Eqs. (20) and (21)], Eq. (39) can be written as

$$Nu = -\frac{1}{A}\int_0^1 \left(\frac{\partial T}{\partial x}\right)_{x=0} dy \tag{41}$$

Table 5 shows representative numerical results that demonstrate the non-Newtonian effect on the overall Nu. The results indicate that $Nu \to 1$ (conduction values) as $Ra \to 0$ for all values of n. This clearly implies that the effect of the power-law index on the overall heat transfer is negligible in the conduction flow regime. However, with an increase in Ra, the magnitude of the overall Nu for any n, branches out from the Newtonian values. The smaller the value of n, the earlier this branching occurs.

This finding can be observed clearly from Fig. 12, where the overall Nu vs Ra is plotted for $A = 1.0$ and $n = 1.0$, 0.8, 0.7, and 0.55. For all cases, Nu approaches the conduction value, $Nu = 1.0$, when $Ra \to 0$. However, the higher the power-law index, the larger the Ra required for Nu to branch out from the Newtonian values.

From the results presented in Table 5 and Fig. 12 it can be seen that for any fixed values of Ra and A, the overall Nu decreases when n increases. Thus, the effect of increasing the power-law index is similar to that of decreasing Ra.

Conclusions

Employing the Darcy model, theoretical and numerical studies of steady-state natural convection fluid flow and heat transfer in a porous medium filled with a non-Newtonian fluid were made. The theoretical solution was constructed along the lines of scale analysis published for Darcy flow of Newtonian fluids by Poulikakos and Bejan.[14] A scale analysis of the modified Darcy formulation leads to three governing parameters for the steady-state natural convection: 1) Ra, 2) AR, and 3) n. The results from the scale analysis provide criteria for the four heat transfer regimes that may arise in the system: 1) pure conduction, 2) tall layers, 3) high Ra convection, and 4) shallow layers.

The natural convection phenomenon discussed on the basis of scaling arguments is verified by numerical experiments. A computer program based on the control volume formulation was used to perform the numerical experiments.

Numerical experiments conducted for $A = 0.5$, 1.0, and 2.0, $Ra = 1.0$, 50.0, and 100 confirmed the scaling predictions. The dependence of Nu on the governing parameters, Ra and n, have also been studied. It has been found that the overall Nu decreases with an increase in n, the reduction being larger at higher Ra. Furthermore, in the limit $Ra \to 0$, the Nu tends to unity for all n. For a fixed value of n, the present results indicate that the heat transfer rate increases with an increase in Ra. Thus, it is concluded that both increasing Ra or decreasing n have similar qualitative effects on the heat transfer.

To our knowledge, there are no experiments to elucidate the heat transfer characteristics of the non-Newtonian fluid flow in a confined porous medium. Thus, experimental work in porous media saturated with power-law fluids needs to be performed and rigorous measurements of velocity and temperature fields as well as the heat transfer coefficients need to be carried out to verify the theoretical results discussed in this article. It is hoped that the work presented in this article will serve as a stimulant to initiate further research activities in the area of transport phenomena in confined porous media saturated with non-Newtonian fluids.

Acknowledgment

The authors wish to acknowledge helpful discussions with Guy Lauriat of CNAM, Paris, France.

References

[1]Cheng, P., "Heat Transfer in Geothermal System," *Advances in Heat Transfer*, Vol. 14, Academic, New York, 1978, pp. 1–100.

[2]Chan, B. K. C., Ivey, C. M., and Barry, J. M., "Natural Convection in Enclosed Porous Media with Rectangular Boundary," *Journal of Heat Transfer*, Vol. 81, 1970, pp. 21–26.

[3]Holst, P. H., and Aziz, K., "A Theoretical and Experimental Study of Natural Convection in a Confined Porous Medium," *Canadian*

Journal of Chemical Engineering, Vol. 150, 1972, pp. 232–241.

[4]Barkvall, C. G., "Natural Convective Heat Transfer in Insulated Structures," Division of Building Technology, Lund Inst. of Technology, Rept. 38, Lund, Sweden, 1972.

[5]Hickox, C. E., and Gartling, D. K., "A Numerical Study of Natural Convection in a Horizontal Porous Layer Subjected to an End-to-End Temperature Difference," *Journal of Heat Transfer*, Vol. 26, 1983, pp. 701–708.

[6]Prasad, V., and Kulacki, F. A., "Convective Heat Transfer in a Rectangular Porous Cavity-Effect of Aspect Ratio on Flow Structure and Heat Transfer," *Journal of Heat Transfer*, Vol. 106, 1984, pp. 158–165.

[7]Weber, J. E., "The Boundary-Layer Regime for Convection in a Vertical Porous Layer," *International Journal of Heat and Mass Transfer*, Vol. 18, 1975, pp. 569–573.

[8]Walker, K. L., and Homsy, G. M., "Convection in Porous Cavity," *Journal of Fluid Mechanics*, Vol. 87, 1979, pp. 449–474.

[9]Nield, D. A., and Bejan, A., *Convection in Porous Media*, Springer–Verlag, New York, 1992.

[10]Schneider, K. J., "Investigation on the Influence of Free Thermal Convection on Heat Transfer Through Granular Material," *Proceedings of the 11th International Congress of Refrigeration*, Pergamon, Oxford, England, UK, 1963, pp. 247–253 (Paper 11-14).

[11]Bories, S. A., and Combarnous, M. A., "Natural Convection in a Sloppy Porous Layer," *Journal of Fluid Mechanics*, Vol. 57, 1973, pp. 63–79.

[12]Prasad, V., and Tuntomo, A., "Inertial Effects on Natural Convection in a Vertical Porous Cavity," *Numerical Heat Transfer*, Vol. 11, 1987, pp. 295–320.

[13]Hong, J. T., and Tien, C. L., "Analysis of Thermal Dispersion Effect on Vertical-Plate Natural Convection in Porous Media," *International Journal of Heat and Mass Transfer*, Vol. 30, 1987, pp. 143–150.

[14]Poulikakos, D., and Bejan, A., "Unsteady Natural Convection on a Porous Layer," *Physics of Fluids*, Vol. 26, 1983, pp. 1183–1191.

[15]Tong, T. W., and Subramanian, E., "A Boundary-Layer Analysis for Natural Convection in Vertical Porous Enclosures—Use of the Brinkman-Extended Darcy Model," *International Journal of Heat and Mass Transfer*, Vol. 28, 1985, pp. 563–571.

[16]Lauriat, G., and Prasad, V., "Natural Convection in a Vertical Porous Cavity; a Numerical Study for Brinkman Extended Darcy Formulation," *Journal of Heat Transfer*, Vol. 109, 1987, pp. 688–696.

[17]Beckermann, C., Ramadhyani, S., and Viskanta, R., "Natural Convection Flow and Heat Transfer Between a Fluid Layer and a Porous Layer Inside a Rectangular Enclosure," *Journal of Heat Transfer*, Vol. 109, 1987, pp. 363–370.

[18]Lauriat, G., and Prasad, V., "Non-Darcian Effects on Natural Convection in a Vertical Porous Enclosure," *International Journal of Heat and Mass Transfer*, Vol. 32, 1989, pp. 2135–2148.

[19]Nield, D. A., "The Limitation of the Brinkman-Forchheimer Equation in Modeling Flow in a Saturated Porous Medium and at an Interface," *International Journal of Heat and Fluid Flow*, Vol. 12, 1970, pp. 269–272.

[20]Bian, W., Vasseur, P., and Bilgen, E., "Boundary-Layer Analysis for Natural Convection in a Vertical Porous Layer Field with a Non-Newtonian Fluid," *International Journal of Heat and Fluid Flow*, Vol. 15, 1994, pp. 384–391.

[21]Bian, W., Vasseur, P., and Bilgen, E., "Natural Convection of Non-Newtonian Fluids in an Inclined Porous Layer," *Chemical Engineering Communication*, Vol. 1129, 1994, pp. 79–97.

[22]Chen, H. T., and Chen, C. K., "Free Convection Flow of Non-Newtonian Fluids Along a Vertical Plate Embedded in a Porous Medium," *Journal of Heat Transfer*, Vol. 110, 1988, pp. 257–260.

[23]Chen, H. T., and Chen, C. K., "Natural Convection of a Non-Newtonian Fluid About a Horizontal Cylinder and a Sphere in a Porous Medium," *International Communications in Heat and Mass Transfer*, Vol. 15, 1988, pp. 605–614.

[24]Chen, H. T., and Chen, C. K., "Natural Convection of Non-Newtonian Fluid About a Horizontal Surface in a Porous Medium," *Journal of Energy Resources Technology*, Vol. 109, 1987, pp. 119–123.

[25]Nakayama, A., "Integral Method for Forced Convection Heat Transfer in Power Law Non-Newtonian Fluids," *Encyclopedia of Fluid Mechanics*, Vol. 1, Gulf Publishing Co., Houston, TX, 1986, pp. 305–339.

[26]Nakayama, A., and Koyama, H., "Buoyancy-Induced Flow of Non-Newtonian Fluid over a Non-Isothermal Body of Arbitrary Shape in a Fluid-Saturated Porous Medium," *Applied Science Research*, Vol. 48, 1991, pp. 55–70.

[27]Nakayama, A., "Free Convection from a Horizontal Line Heat Source in a Power-Law Fluid Saturated Porous Medium," *International Journal of Heat and Fluid Flow*, Vol. 14, 1993, pp. 279–282.

[28]Pop, I., and Nakayama, A., "Conjugate Free Convection from Long Vertical Plate Fins in a Non-Newtonian Fluid Saturated Porous Medium," *International Communications in Heat and Mass Transfer*, Vol. 21, 1994, pp. 297–305.

[29]Shanoy, A., "Non-Newtonian Fluid Heat Transfer in Porous Media," *Advances in Heat Transfer*, Vol. 24, Academic, New York, 1994, pp. 101–190.

[30]Getachew, D., Minkowycz, W. J., and Poulikakos, D., "Constitutive Equations of Non-Newtonian Fluids in a Porous Matrix," *Journal of Non-Newtonian Fluid Mechanics* (submitted for publication).

[31]Getachew, D., "Non-Newtonian Convection in a Porous Matrix: Constitutive Equations and an Application," Ph.D. Dissertation, Univ. of Illinois at Chicago, IL, 1994.

[32]Bejan, A., *Convection Heat Transfer*, Wiley, New York, 1984.

[33]Patankar, S. V., *Numerical Heat Transfer and Fluid Flow*, Hemisphere, Washington, DC, 1980.

[34]Patankar, S. V., *Computation of Conduction and Duct Flow Heat Transfer*, Innovative Research, Inc., Maple Grove, MN, 1991.

[35]Patankar, S. V., "Elliptic Systems: Finite Difference Method I," *Handbook of Numerical Heat Transfer*, edited by W. J. Minkowycz, E. M. Sparrow, G. E. Schneider, and R. H. Pletcher, Wiley, New York, 1988.

[36]Roache, P. J., *Computational Fluid Dynamics*, Hermosa, Albuquerque, NM, 1972.